Structural, Magnetic, and Electronic Properties of Vanadium-Substituted Nickel Chromium Sulfide

Paz Vaqueiro,[†] Markus Bold,[†] Anthony V. Powell,*[,†] and Clemens Ritter[‡]

Department of Chemistry, Heriot-Watt University, Riccarton, Edinburgh EH14 4AS, United Kingdom, and Institut Max Von Laue-Paul Langevin, F-38042 Grenoble, France

Received September 30, 1999. Revised Manuscript Received January 26, 2000

A series of sulfides $NiCr_{2-x}V_xS_4$ ($0 < x < 2.0$) has been synthesized at high temperatures. All products are isostructural with Cr_3S_4 (space group $I2/m$; $a \approx 5.9$ Å, $b \approx 3.4$ Å, $c \approx 11.1$ Å; $\beta \approx 91.8°$) in which octahedral sites between pairs of close-packed anion layers are alternately fully and half occupied. Materials with $x < 0.6$ are variable-range-hopping semiconductors, whereas those with higher vanadium contents are metallic. The insulator to metal transition at $x \approx 0.6$ is accompanied by a structural distortion, which results in the formation of cation chains in the fully occupied layer. Magnetic susceptibility data indicate that magnetic order initially persists into the metallic phase, disappearing above $x = 0.8$. Powder neutron diffraction data reveal that the magnetic order involves a doubling of the crystallographic unit cell in both the *a* and *c* directions.

Introduction

Many ternary transition metal sulfides of stoichiometry AB_2S_4 adopt the monoclinic Cr_3S_4 structure.[1−5] This is an ordered defect structure[6] intermediate between the NiAs and CdI_2 types. In the former, cations occupy all of the octahedral sites between pairs of hexagonally close packed anion layers. The removal, in an ordered manner, of 50% of the cations in alternate cation layers gives rise to the Cr_3S_4 structure. This may be viewed as consisting of layers of edge-shared octahedra, of stoichiometry MS_2, separated by partially occupied layers in which vacancy ordering produces a two-dimensional superstructure. Cations in this layer share a common octahedral face with those in the neighboring layers. The presence of two crystallographically distinct cation sites (Figure 1), suggests that ternary phases AB_2S_4 may show one of two extreme cation arrangements. In the normal structure, the A cations reside exclusively in the vacancy layer, whereas in the inverse structure, half of the B cations occupy vacancy layer sites and A cations reside exclusively in the fully occupied layer. Cation partitioning is, however, seldom complete,[7−10] and recent studies,[11−13] have shown that the distribution is dependent on the electronic properties of the constituent cations. In particular, cations drawn from the early part of the transition series show

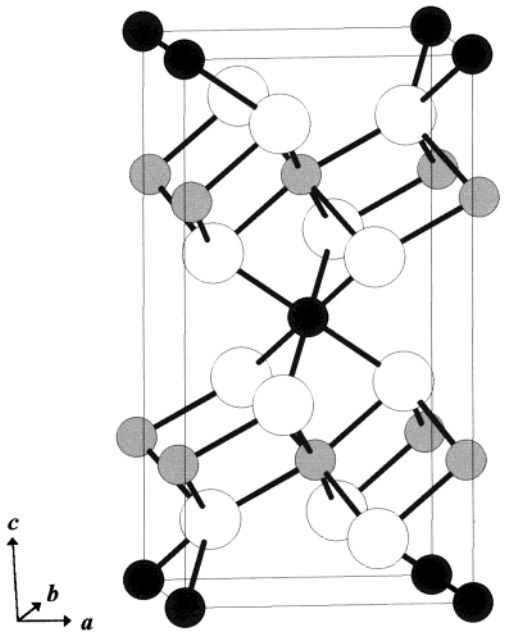

Figure 1. A ball-and-stick representation of the Cr_3S_4 structure. Large open circles represent anions, small black circles represent cations in the vacancy layer, and small gray circles represent cations in the fully occupied layer.

* To whom correspondence should be addressed. Fax: +44 (0)131 451 3180. E-mail: A.V.Powell@hw.ac.uk.
[†] Heriot-Watt University.
[‡] Institut Max Von Laue-Paul Langevin.

(1) Wold, A.; Dwight, K. In *Solid State Chemistry: Synthesis, Structure and Properties of Selected Oxides and Sulfides*; Chapman and Hall: New York, 1993.
(2) Plovnick, R. H.; Perloff, D. S.; Vlasse, M.; Wold, A. *J. Phys. Chem. Solids* **1968**, *29*, 1935.
(3) Murugesan, T.; Ramesh, S.; Gopalakrishnan, J.; Rao, C. N. R. *J. Solid State Chem.* **1982**, *44*, 119.
(4) Chevrel, R.; Sergent, M.; Meury, J. L.; Quan, D. T.; Colin, Y. *J. Solid State Chem.* **1974**, *10*, 260.
(5) Morris, B. L.; Plovnick, R. H.; Wold, A. *Solid State Commun.* **1969**, *7*, 291.
(6) Jellinek, F. *Acta Crystallogr.* **1957**, *10*, 620.
(7) Hayashi, A.; Ueda, Y.; Kosuge, K.; Murata, H.; Asano, H.; Wanatabe, N.; Izumi, F. *J. Solid State Chem.* **1987**, *71*, 237.
(8) Ueda, Y.; Kosuge, K.; Urabayashi, M.; Hayashi, A.; Kachi, S. *J. Solid State Chem.* **1985**, *56*, 263.
(9) Powell, A. V.; Ritter, C.; Vaqueiro, P. *J. Solid State Chem.* **1999**, *144*, 372.
(10) Newsam, J. M.; Endoh, Y.; Kawada, I. *J. Phys. Chem. Solids* **1987**, *48*, 607.
(11) Powell, A. V.; Colgan, D. C.; Vaqueiro, P. *J. Mater. Chem.* **1999**, *9*, 485.
(12) Colgan, D. C.; Powell, A. V. *J. Mater. Chem.* **1997**, *7*, 2433.
(13) Colgan, D. C.; Powell, A. V. *J. Mater. Chem.* **1996**, *6*, 1579.

10.1021/cm990613e CCC: $19.00
Published on Web 03/30/2000

a greater preference for sites in the fully occupied layer. This may be related to the ability of such cations to delocalize electron density by direct $t_{2g}-t_{2g}$ interactions.

Although both $NiCr_2S_4$ and NiV_2S_4 adopt the Cr_3S_4 structure, with cation distributions close to the normal type,[11,12] they exhibit contrasting magnetic and electrical properties. Whereas NiV_2S_4 is paramagnetic[11] and metallic,[14] $NiCr_2S_4$ is antiferromagnetic ($T_N = 180$ K) and a low activation energy semiconductor.[15,16] Differences in electronic properties may be traced to the differing nature of the t_{2g} states associated with cations in the fully occupied layer.[17] In NiV_2S_4 the t_{2g} states are broadened by cation−cation interactions into a narrow band, which for V(III):d^2 is partially filled. In the chromium analogue, the Fermi energy is raised and weaker cation−cation interactions result in band narrowing and greater localization of t_{2g} states. Consequently, as chromium is progressively substituted by vanadium, a semiconductor to metal transition is anticipated. Substitution creates holes in the t_{2g}-derived band which the rigid band model suggests would lead to metallic conduction in nonstoichiometric phases. By preparing the series $NiCr_{2-x}V_xS_4$, we sought to investigate systematically changes in structural and physical properties as the level of vanadium substitution is varied. Contrary to the predictions of the rigid-band model,[17] which implies metallic behavior for all nonstoichiometric materials, a critical level of doping ($x_c \approx 0.6$) is required before the insulator to metal transition is observed. This is accompanied by structural changes in the fully occupied layer, a preliminary account of which has recently been communicated.[18] Moreover, complex changes in the magnetic properties occur with an increasing level of doping. In this work a detailed account of the structural, magnetic, and electronic properties of $NiCr_{2-x}V_xS_4$ is presented.

Experimental Section

Materials were synthesized from the elements by firing at elevated temperatures. Samples were prepared with a slight deficiency of sulfur, corresponding to a composition of $NiCr_{2-x}V_xS_{3.93}$, as previous studies[6] have shown that the phase range of the Cr_3S_4 structure does not extend to the fully stoichiometric composition. Mixtures of nickel (Goodfellow, 99.5%), chromium (Aldrich, 99%), vanadium (Aldrich, 99.5%), and sulfur (Aldrich, 99.9%) with the appropriate stoichiometry were ground in an agate mortar prior to sealing into evacuated ($<10^{-4}$ Torr) silica tubes. Mixtures were fired at 800 °C for a period of between 9 and 17 days with intermediate regrinding. Samples were cooled to 300 °C at ~2 °C min^{-1} prior to removal from the furnace.

Powder X-ray diffraction data were collected with a Philips PA2000 diffractometer using nickel-filtered Cu Kα radiation. Data were collected in step-scan mode using a step size of 0.02°(2θ) and a counting time of 5 s $step^{-1}$. Energy-dispersive microanalysis was performed with a Hitachi S2700 scanning electron microscope equipped with a PGT IMIX-XE analysis system. Ni, Cr, V, and CdS were used as intensity standards.

The electrical resistance of the samples was measured using the four-probe dc technique. An ingot (~6 × 3 × 1 mm) was cut from a sintered pellet, four 50 μm silver wires were attached using colloidal silver paint and connections were made to a HP34401A multimeter. The sample was mounted in an Oxford Instruments CF1200 cryostat connected to an ITC502 temperature controller. Measurements were carried out over the temperature range $77 \le T/K \le 300$. For compositions in the range $0.1 \le x \le 0.6$ measurements were extended to 6 K. Magnetic measurements were performed using a Quantum Design MPMS2 SQUID susceptometer. Samples were loaded into gelatin capsules at room temperature. Data were collected over the temperature range $4 \le T/K \le 300$, both after cooling in zero applied field (zfc) and after cooling in the measuring field (fc) of 1000 G. Data were corrected for the diamagnetism of the gelatin capsule and for intrinsic core diamagnetism.

Powder neutron diffraction data were collected at room temperature on the D2B diffractometer ($\lambda = 1.59379$ Å) at ILL, Grenoble. Samples (~3 g) were contained in a vanadium can and patterns were recorded over the range $10 \le 2\theta/deg \le 160$ over a period of 3 h. For compositions with $x \le 0.6$, data were also collected over the temperature range $1.3 \le T/K \le 293$ in increments of ~10 K, on the D1B diffractometer ($\lambda = 2.524$ Å) also at ILL. Additional low-temperature data were collected using the Polaris diffractometer at the ISIS spallation source, Rutherford Appleton Laboratory. All Rietveld refinements were performed with the GSAS package[19] installed on the Heriot-Watt University Alpha 2100−4275 system.

Results

Powder X-ray diffraction patterns could be indexed on the basis of a monoclinic unit cell similar to that of Cr_3S_4. Data indicate that with the exception of $NiCr_{1.9}V_{0.1}S_4$, all materials are single phases. An extra reflection ($d = 2.83$ Å) which may be assigned to NiS_2 ($d_{200} = 2.83$ Å)[20] was observed in the pattern of $NiCr_{1.9}V_{0.1}S_4$. Microanalysis indicates that the samples are homogeneous and experimentally determined compositions (Table 1) are in good agreement with the stoichiometry of the initial reaction mixtures.

Examination of the magnetic susceptibility data revealed three distinct types of magnetic behavior; representative data for which are shown in Figure 2. The behavior of materials with compositions in the range $0 \le x \le 0.8$ (Figure 2a) is similar to that of $NiCr_2S_4$.[15,21] On cooling, fc and zfc data pass through a local maximum, the temperature of which (76−145 K) is composition dependent. Data at temperatures above this maximum do not follow Curie−Weiss behavior. The local maximum in susceptibility is associated with the onset of long-range magnetic order. Low-temperature neutron diffraction confirmed that the nature of the magnetic order is similar to that in the stoichiometric phase and also demonstrated the absence of magnetic order in samples with $x > 0.8$. An increase in measured susceptibility at lower temperatures suggests that some spontaneous magnetization remains in the complex magnetically ordered state. At higher doping levels, there is a marked increase in the magnitude of the susceptibility at low temperatures. Compositions over the range $1.0 \le x \le 1.4$ (Figure 2b) show a broad maximum at low temperatures, below which zfc and fc

(14) Bouchard, R. J.; Wold, A. *J. Phys. Chem. Solids* **1966**, *27*, 591.
(15) Morris, B. L.; Russo, P.; Wold, A. *J. Phys. Chem. Solids* **1970**, *31*, 635.
(16) Powell, A. V.; Colgan, D. C.; Ritter, C. *J. Solid State Chem.* **1997**, *134*, 110.
(17) Holt, S. L.; Bouchard, R. J.; Wold, A. *J. Phys. Chem. Solids* **1966**, *27*, 755.
(18) Powell, A. V.; Vaqueiro, P. *Chem. Commun.* **1999**, 753.
(19) Larson, A. C.; von Dreele, R. B. *General Structure Analysis System*; Los Alamos Laboratory Report LAUR 86-748; Los Alamos Laboratory: Los Alamos, NM, 1994.
(20) JCPDS PDF card no 11-99, Joint commitee on Powder Diffraction Standards, Swarthmore, PA.
(21) Tressler, R. E.; Stubican, V. S.; *J. Am. Ceram. Soc.* **1968**, *51*, 393.

Table 1. Results of Thermogravimetric Analysis and Energy-Dispersive X-ray Microanalysis for $NiCr_{2-x}V_xS_4$ ($0 < x < 2$) Phases

nominal composition	reaction time,days	Ni:Cr		Ni:V		Ni:S		experimental composition[a]
		nominal	experimental	nominal	experimental	nominal	experimental	
$NiCr_{1.9}V_{0.1}S_{3.93}$	15	0.53	0.48(4)	10	11(1)	0.254	0.23(3)	$Ni_{0.95}Cr_{1.97}V_{0.09}S_{4.1}$[b]
$NiCr_{1.8}V_{0.2}S_{3.93}$	11	0.56	0.54(3)	5	5.0(8)	0.254	0.25(2)	$Ni_{0.98}Cr_{1.82}V_{0.20}S_{3.93}$
$NiCr_{1.7}V_{0.3}S_{3.93}$	13	0.59	0.53(2)	3.33	3.00(8)	0.254	0.23(3)	$Ni_{0.93}Cr_{1.76}V_{0.31}S_{4.05}$
$NiCr_{1.6}V_{0.4}S_{3.93}$	13	0.63	0.60(3)	2.5	2.5(1)	0.254	0.25(2)	$Ni_{0.98}Cr_{1.63}V_{0.39}S_{3.90}$
$NiCr_{1.5}V_{0.5}S_{3.93}$	8	0.67	0.64(1)	2.0	2.0(1)	0.254	0.25(1)	$Ni_{0.98}Cr_{1.53}V_{0.49}S_{3.92}$
$NiCr_{1.4}V_{0.6}S_{3.93}$	12	0.71	0.65(2)	1.67	1.6(1)	0.254	0.24(3)	$Ni_{0.95}Cr_{1.46}V_{0.60}S_{3.95}$
$NiCr_{1.2}V_{0.8}S_{3.93}$	14	0.83	0.79(2)	1.25	1.3(6)	0.254	0.25(2)	$Ni_{0.99}Cr_{1.25}V_{0.76}S_{3.95}$
$NiCr_{1.0}V_{1.0}S_{3.93}$	17	1.0	0.87(4)	1.0	0.94(6)	0.254	0.24(2)	$Ni_{0.93}Cr_{1.07}V_{0.99}S_{3.90}$
$NiCr_{0.8}V_{1.2}S_{3.93}$	17	1.25	1.08(2)	0.83	0.81(2)	0.254	0.25(2)	$Ni_{0.95}Cr_{0.88}V_{1.17}S_{3.80}$
$NiCr_{0.6}V_{1.4}S_{3.93}$	9	1.67	1.43(6)	0.71	0.72(6)	0.254	0.24(2)	$Ni_{0.97}Cr_{0.68}V_{1.35}S_{4.05}$
$NiCr_{0.2}V_{1.8}S_{3.93}$	12	5	4.1(8)	0.56	0.52(1)	0.254	0.24(1)	$Ni_{0.95}Cr_{0.23}V_{1.82}S_{4.00}$

[a] Normalized to a total metal content of three. [b] Sample also contains NiS_2.

data diverge, suggesting a magnetically frustrated system. The maximum in susceptibility may be identified with a spin-glass transition ($T_g = 5-15$ K). The glass transition temperature, T_g, decreases with vanadium doping. At higher levels of doping ($x > 1.4$), paramagnetism is observed down to the lowest temperatures studied, although the possibility of a glass transition below 4 K cannot be excluded. Zfc data for all materials in the range $1.0 \le x < 2.0$ can be described by a modified Curie−Weiss law of the form $\chi = \chi_0 + C/(T - \theta)$, where χ_0 is a temperature-independent paramagnetic term. Derived magnetic parameters are presented in Table 2.

Electrical data for compositions $0.8 \le x < 2.0$ show very low, almost temperature-independent, resistivities. The positive sign of $d\rho/dT$ is indicative of metallic behavior. By contrast, the resistivity for materials over the range $0.0 < x \le 0.5$ increases on cooling, consistent with semiconducting behavior. Representative data for each composition region are shown in Figure 3a. For compositions between these two regions ($0.5 < x < 0.8$), there is some ambiguity over the sign of $d\rho/dT$. For example, for $NiCr_{1.4}V0.6S_4$ $d\rho/dT$ is small and positive down to ~40 K, which is consistent with metallic behavior, but on further cooling the resistivity shows a slight increase. This may reflect the dominance of grain boundary resistances, arising from the polycrystalline nature of the materials, at lower temperatures. For materials in the semiconducting regime, plots of $\ln(\rho)$ vs $1/T$ are nonlinear indicating that the conduction mechanism is not of the Arrhenius type. However, the data conform to a variable-range-hopping model[22] of the form

$$\rho = \rho_0 \left(\frac{T}{T_0}\right)^{1/2} \exp\left[\left(\frac{T_0}{T}\right)^{\nu}\right] \qquad (1)$$

where the exponent ν is $^1/_4$ for a three-dimensional conduction and $^1/_3$ for a two-dimensional conduction. Plots of $\ln(\rho/T^{1/2})$ vs $T^{-1/4}$ or $T^{-1/3}$ are linear over a wide range of temperatures (Figure 3b). The temperature range over which the fits were performed, together with the resulting parameters for $\nu = {}^1/_4$, are presented in Table 3.

Room-Temperature Neutron Data. Rietveld refinements, using room-temperature X-ray and neutron diffraction data simultaneously, were used to establish the distribution of cations between the two crystallographic sites. Refinements were initiated in the space group $I2/m$, using a structural model, obtained from X-ray data alone, in which nickel solely occupies the vacancy layer (2a) sites. Following refinement of scale factors, background terms, instrumental, lattice, positional, thermal, and pseudo-Voigt peak-shape parameters, cation site occupancy factors were introduced as variables into the refinement. Two different structural models were considered: the site occupancy factor of nickel at each of the two crystallographic sites was allowed to vary together with those of *either* chromium or vanadium, with the constraint that overall stoichiometry was maintained. In both models, refinement of site occupancy factors resulted in comparable reductions (~6%) in weighted residuals. However, the fraction of vanadium in the vacancy layer site in NiV_2S_4 is very low (<3%) and vanadium cations show a marked preference for sites in the fully occupied layer.[11] Therefore, the model in which vanadium resides exclusively in the fully occupied layer was preferred for the refinement of the magnetic structures.

Final, observed, calculated, and difference profiles for $NiCr_{1.8}V_{0.2}S_4$ are given in Figure 4. Structural refinements for other compositions are of similar quality ($R_{wp} = 3-7\%$) and profiles are provided as Supporting Information together with the refined structural parameters. The compositional dependence of lattice parameters, unit cell volume and important cation−cation distances are summarized in Figure 5. The a and b parameters, together with the volume, decrease with increasing vanadium substitution, whereas the angle β increases The c parameter varies by ≤0.3% across the series.

Low-Temperature Neutron Data. Neutron data collected at 1.3 K for materials in the composition range $0 < x \le 0.6$ exhibit additional magnetic Bragg peaks. This indicates a doubling of the unit cell in the a and c directions similar to that observed for $NiCr_2S_4$, the magnetic structure of which was used for the trial magnetic structure of the vanadium-doped phases. The free-ion form factors[23] for Ni^{2+} and Cr^{3+} were used to describe the angular dependence of the magnetic scattering (V^{3+} was not considered because of the low degree of doping). Site occupancy factors were fixed at the values determined at room temperature and an overall thermal parameter was used. A region centered at 2θ

(22) Shklovskii, B. I.; Efros, A. L. In *Electronic properties of Doped Semiconductors*; Springer-Verlag: Berlin, 1984.
(23) Brown, P. J. In *International Tables for Crystallography*; Wilson, A. J. C., Ed.; Kluwer: Dordrecht, 1992; Vol. C, Chapter 4.

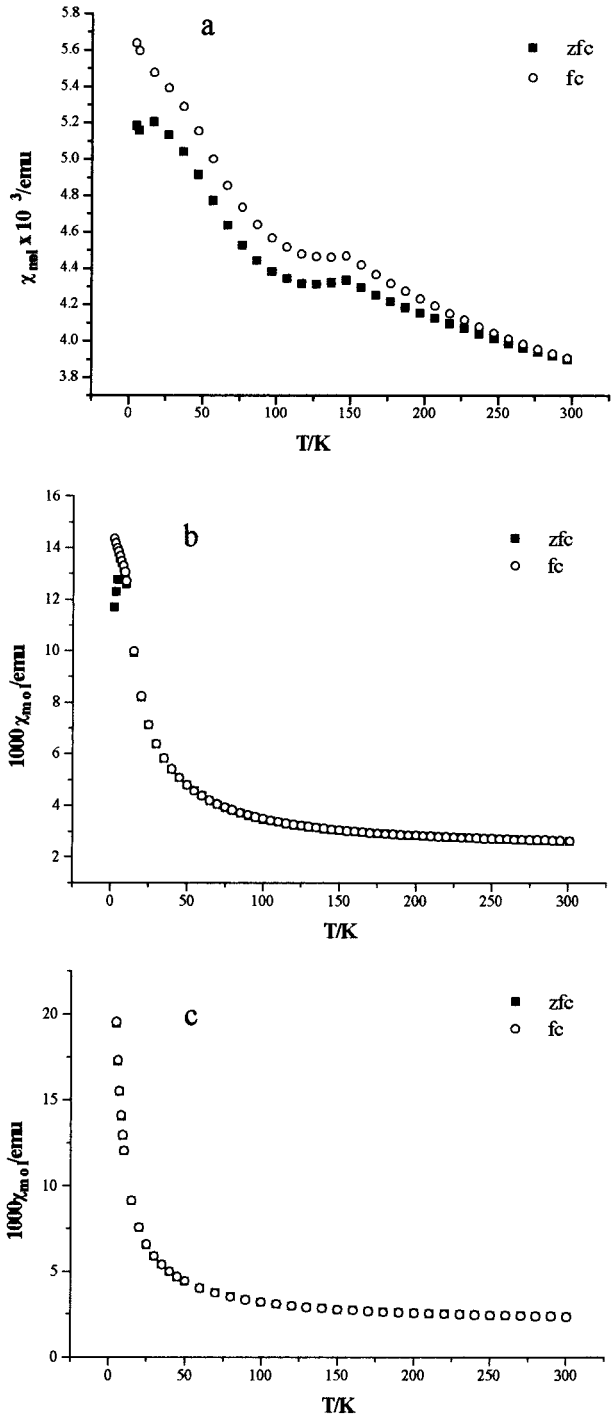

Figure 2. Zero-field-cooled (zfc) and field-cooled (fc) molar magnetic susceptibilities for (a) $NiCr_{1.6}V_{0.4}S_4$, (b) $NiCr_{0.8}V_{1.2}S_4$, and (c) $NiCr_{0.6}V_{1.4}S_4$.

Table 2. Parameters Derived from Magnetic Susceptibility Data Using a Modified Curie−Weiss Expression

x	data range, K	χ_0, emu	C, emu K	θ, K	μ_{exp}(Ni)
1.8	10−210	$1.24(1) \times 10^{-3}$	0.074(1)	−5.1(3)	0.77
1.4	10−300	$1.94(7) \times 10^{-3}$	0.129(1)	−2.8(1)	1.02
1.2	20−300	$2.15(6) \times 10^{-3}$	0.138(1)	−2.6(1)	1.05
1.0	30−300	$2.32(7) \times 10^{-3}$	0.174(1)	−1.2(2)	1.18

= 72.7° was excluded from the refinement due to the presence of an instrumental feature. For the material $NiCr_{1.9}V_{0.1}S_4$ a region centered at 2θ = 53° was also excluded, because of the occurrence of a peak due to

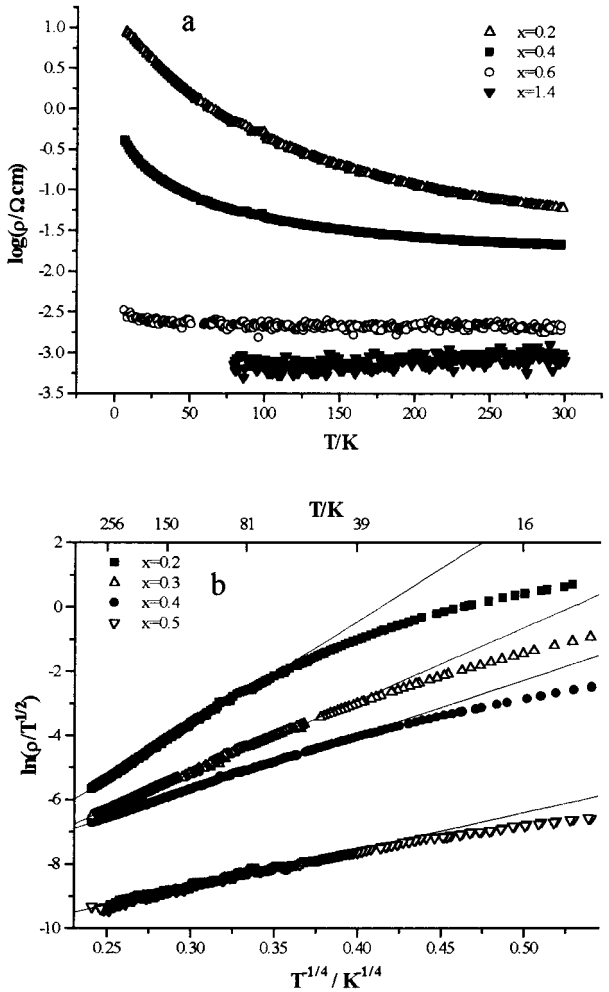

Figure 3. Electrical data for representative compositions along the series $NiCr_{2-x}V_xS_4$: (a) temperature dependence of the electrical resistivity; (b) $T^{-1/4}$ dependence of ln(ρ). The straight lines are the fit to the variable-range-hopping expression over the range of temperatures given in Table 3.

Table 3. Parameters Extracted from Variable-Range-Hopping Fits with $\nu = 1/4$

compound	T, K	ρ_0, 10^{-3} Ωcm	T_0, 10^4 K	ξ, Å
$NiCr_{1.9}V_{0.1}S_{3.93}$	165−77	0.501	417	0.71
$NiCr_{1.8}V_{0.2}S_{3.93}$	300−68	1.24	125	1.1
$NiCr_{1.7}V_{0.3}S_{3.93}$	300−43	3.14	27.1	1.8
$NiCr_{1.6}V_{0.4}S_{3.93}$	300−36	5.75	8.61	2.6
$NiCr_{1.5}V_{0.5}S_{3.93}$	300−35	0.719	1.64	4.5

NiS_2. Initial refinement of magnetic vector components suggested that only μ_x(M), μ_z(M), and μ_x[M], where parentheses and square brackets represent sites in the vacancy and fully occupied layers respectively, were nonzero and the remaining components were therefore constrained at zero. Final observed, calculated, and difference profiles for the material $NiCr_{1.8}V_{0.2}S_4$ are given in Figure 6; those for other compositions which are of similar quality (R_{wp} = 1−3%), are provided as Supporting Information. The compositional dependence of the moments associated with cations at the two sites is shown in Figure 7.

Variable-Temperature Neutron Diffraction Data. The thermal evolution of the diffraction pattern of $NiCr_{1.8}V_{0.2}S_4$ is shown in Figure 8. All phases in the range $0 < x \leq 0.6$ show similar behavior, with the magnetic ordering temperature, determined from a plot

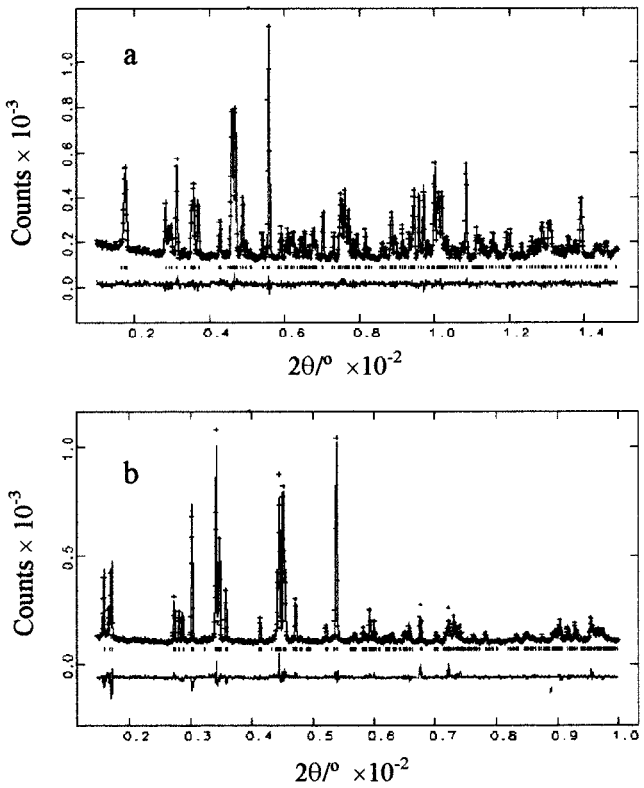

Figure 4. Observed (crosses), calculated (upper full line), and difference (lower full line) profiles for $NiCr_{1.8}V_{0.2}S_4$ at room temperature: (a) neutron data and (b) X-ray data. Reflection positions are marked.

of the intensity of the ($^1/_2$,0,$^3/_2$) reflection as a function of temperature, decreasing with increasing vanadium doping (Figure 9). Lattice parameters for all phases in this composition region show similar behavior with temperature (Figure 10). Both *a* and *c* decrease, with decreasing temperature, whereas *b* is approximately temperature independent. The monoclinic distortion increases on cooling.

Discussion

Solid−solution behavior is found across the entire $NiCr_{2-x}V_xS_4$ series and a near normal cation distribution is adopted throughout. This is consistent with our conclusions from a number of studies on Cr_3S_4-type systems.[11−13] There is no evidence of ordering of vanadium and chromium cations in the fully occupied layer. All cations have a distorted octahedral coordination. Those in the fully occupied layer show an increase in the extent of this distortion with increasing vanadium content, as reflected in the range of bond angles which changes from 83−95° in $NiCr_{1.9}V_{0.1}S_4$ to 79−102° in $NiCr_{0.2}V_{1.8}S_4$.

Vanadium doping induces structural changes in the fully occupied layer. In $NiCr_2S_4$ each cation in the fully occupied layer has six nearest-neighbor cations in a pseudohexagonal arrangement within the layer (Figure 11a). Rietveld refinement using the room-temperature data for $NiCr_{1.9}V_{0.1}S_4$ showed that there are two neighbors at ∼3.4 Å (r_1) resulting from lattice translation along the *b* axis, two at a short distance (r_2) of ∼3.2 Å and two at a slightly greater separation (r_3) of ∼3.6 Å. At low levels of vanadium doping this geometry is little

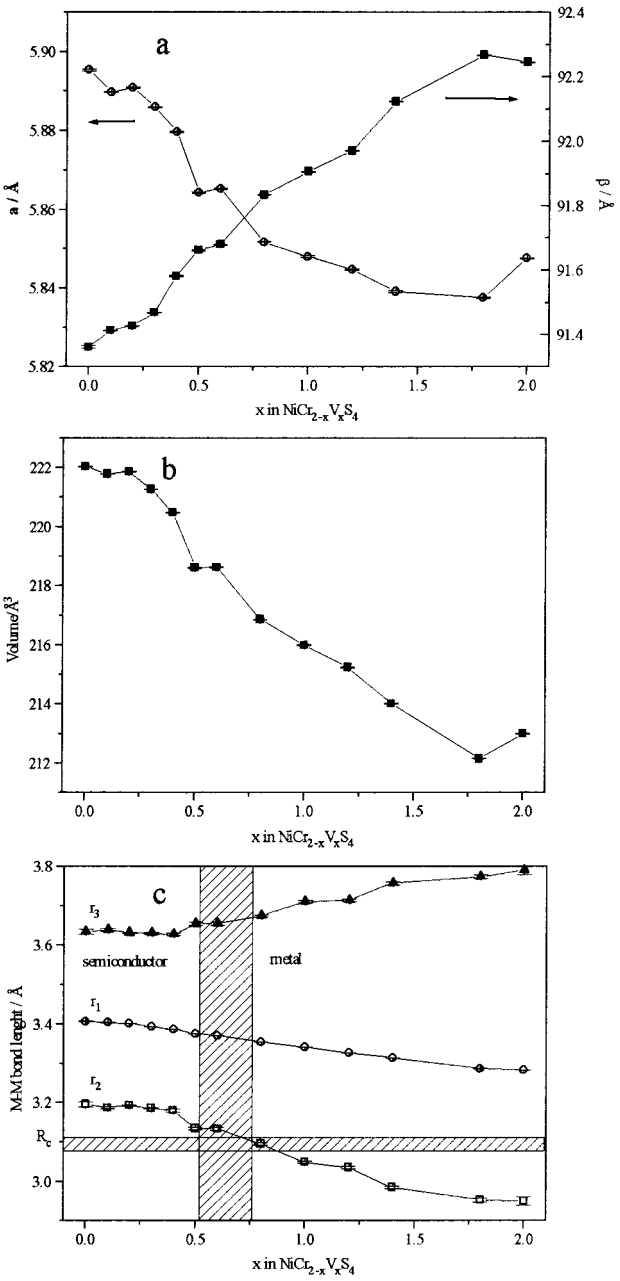

Figure 5. Composition dependence of (a) the lattice parameters, (b) the unit cell volume, and (c) metal−metal distances in the fully occupied layer. Data for $x = 0$ and $x = 2$ phases are taken from refs 16 and 11, respectively.

perturbed. However, while r_1 exhibits little change over the entire compositional range, above $x = 0.4$, r_3 increases and r_2 decreases (Figure 5c). This produces a discontinuity in the ratio r_3/r_2 at $x \approx 0.5$ (Figure 12) in the region of composition where the change from a magnetically ordered semiconductor to a magnetically ordered metal is observed. Below this critical doping level, r_3/r_2 is effectively invariant at ∼1.1, whereas above $x = 0.5$ it increases markedly. The increase in r_3/r_2 is reflected in a structural change, resulting in the formation of cation chains directed along [010] (Figure 11), in which the intrachain cation−cation separation (r_2) is considerably shorter than the shortest interchain (r_3) distance. These distances are ∼2.9 and ∼3.8 Å, respectively in NiV_2S_4. For V(III) and Cr(III) an empirical estimate[24] for the critical distance, R_c, for direct $t_{2g}-t_{2g}$

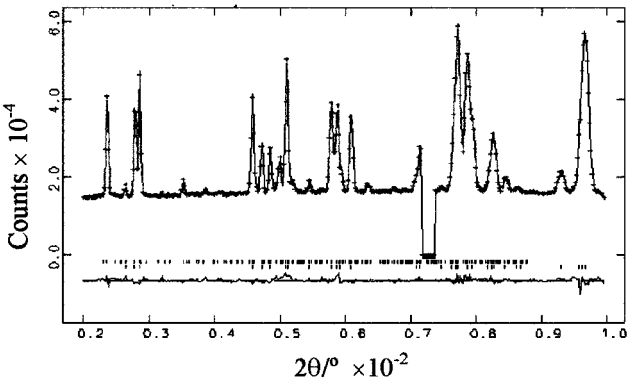

Figure 6. Observed (crosses), calculated (upper full line), and difference (lower full line) neutron diffraction profiles for $NiCr_{1.8}V_{0.2}S_4$ at 1.3 K. Reflection positions are marked. The lower markers refer to the crystallographic unit cell and the upper markers to the magnetic unit cell described in the primitive space group P1.

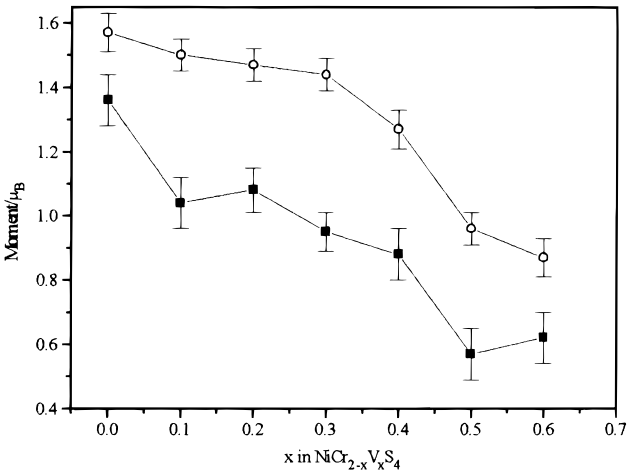

Figure 7. Composition dependence of the ordered moments associated with cations at sites in the vacancy layer (■) and in the fully occupied layer (□). Data for the $x = 0$ phase are taken from ref 16.

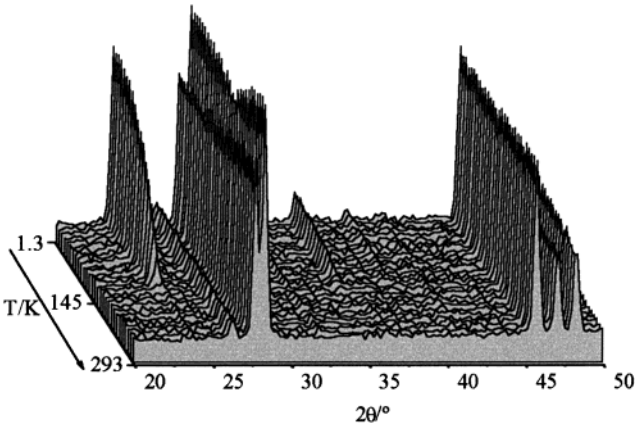

Figure 8. Powder neutron diffraction data for $NiCr_{1.8}V_{0.2}S_4$ over the temperature range $1.3 \leq T/K \leq 293$.

orbital overlap is ~3.1 Å. For compositions with $x > 0.6$, the metal−metal distance in the zigzag chains is below this critical distance. This would give rise to a one-dimensional band, which at these levels of doping is

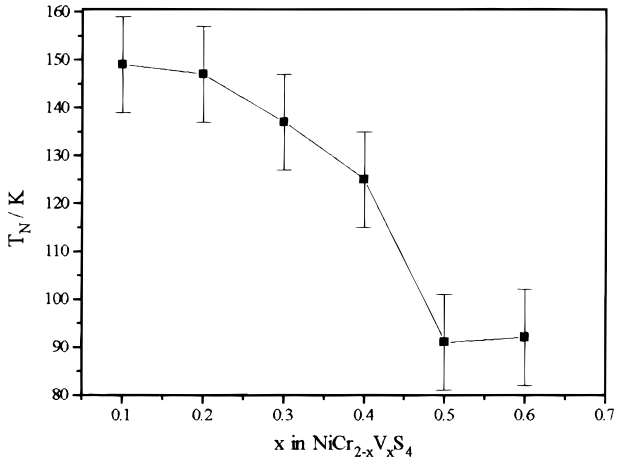

Figure 9. Composition dependence of the magnetic ordering temperature.

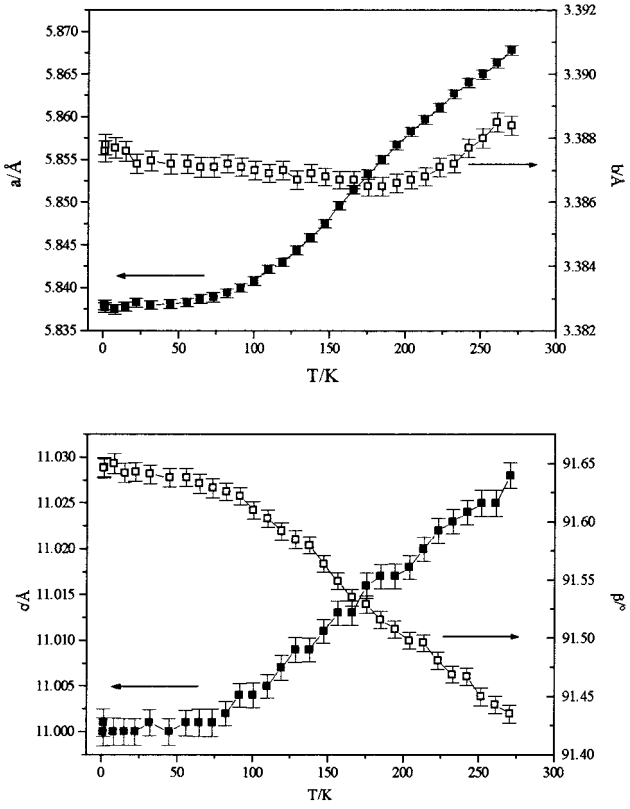

Figure 10. Temperature dependence of the unit cell parameters for $NiCr_{1.8}V_{0.2}S_4$.

partially occupied, leading to the observed metallic behavior. This is supported by the calculations of Canadell et al.,[25] which demonstrate that for an MS_2 layer containing d^2 ions, the zigzag clustering observed here allows strong cation−cation interactions, leading to pronounced dispersion of one component of the t_{2g}-derived band. The itinerant nature of the electrons associated with cations in the fully occupied layer may also account for the significant temperature-independent paramagnetic contribution to the susceptibility of materials in the range $0.5 \leq x < 2.0$. This suggests that the observed effective magnetic moments arise from

(24) Goodenough, J. B. In *Magnetism and the Chemical Bond*; Wiley: New York, 1963.

(25) Canadell, E.; LeBeuze, A.; Abdelaziz El Khalifa, M.; Chevrel, R.; Whangbo, M. H. *J. Am. Chem. Soc.* **1989**, *111*, 3778.

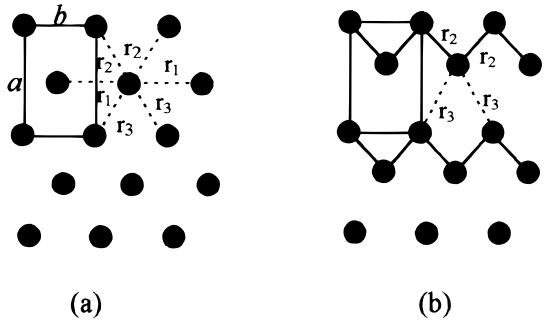

Figure 11. (a) The pseudo hexagonal arrangement of cations in the fully occupied layer in materials with $x \leq 0.4$ and (b) the zigzag chains of cations directed along [010] in materials with $x > 0.4$.

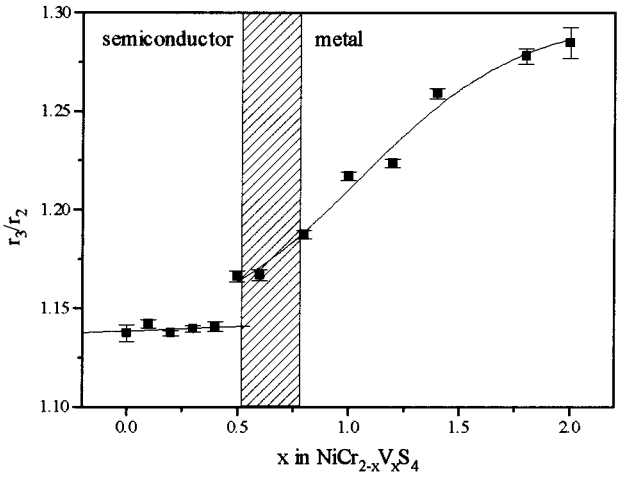

Figure 12. Correlation between the compositional dependence of the degree of distortion within the fully occupied layer and electronic properties.

cations in the vacancy layer, although they exhibit a similar reduction from the spin-only value for Ni(II) (2.82 μ_B) as those in related materials.[26] Similar structural distortions have been reported[11,27] for chalcogenides of stoichiometry MV_2X_4 (M = Ti, V, Fe, Ni; X = S, Se), the electron-transport and magnetic properties of which are consistent with the presence of itinerant electrons in the fully occupied layer, resulting from direct overlap of cation orbitals.

In the semiconducting regime, the one-electron one-molecule energy level diagram for $NiCr_2S_4$[17] shows a filled band due to covalent mixing of anion and e_g nickel orbitals. On substitution of Cr(III):d^3 by V(III):d^2, disorder arising from the randomly distributed cations may cause states at the band edge to become localized, while states in the band center remain delocalized. As the Fermi energy is on the localized side of the mobility edge, the conduction is dominated by hopping of charge carriers between states localized on opposite sides of the Fermi energy according to the variable-range-hopping mechanism. The constant T_0 (Table 3), determined for the compounds in the variable-range-hopping regime (eq 1), is given by[28] $T_0 = 21/k_B N(E_F)\xi^3$, where $N(E_F)$ is the density of states at the Fermi level and ξ is the localization length, which is a measure of the spatial

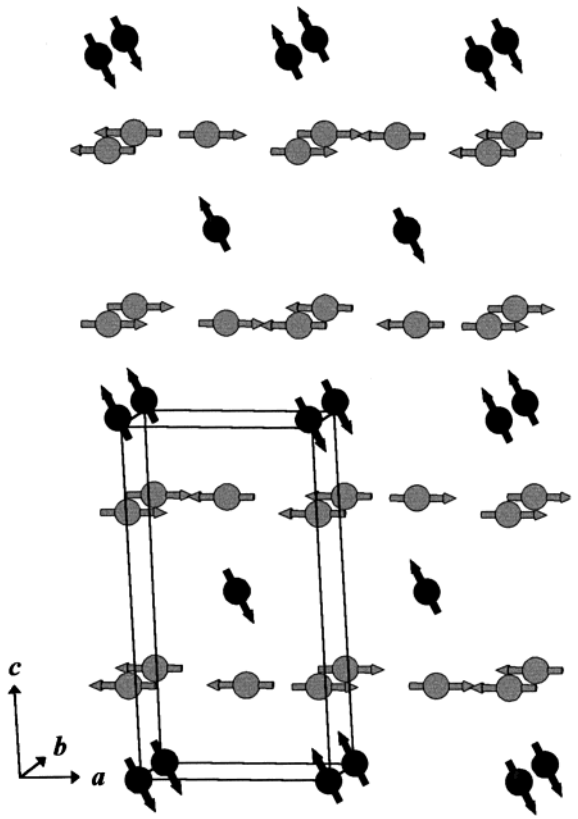

Figure 13. The magnetic structure of $NiCr_{1.8}V_{0.2}S_4$ at 1.3 K.

extent of the wave function localized at a single site. An estimate of ξ was obtained by using a value of $N(E_F) = 1.6 \times 10^{23}$ states/eV cm^3 from band structure calculations for CrS.[29] Divergent behavior of ξ is expected[30] close to the insulator to metal transition and, as shown in Table 3, ξ increases exponentially as the transition is approached.

Materials in the range $0.1 \leq x \leq 0.6$ exhibit long-range magnetic order, the onset of which is marked by a local maximum in the susceptibility. The magnetic structure determined at 1.3 K (Figure 13), for materials in this range of composition, is similar to that of the stoichiometric end-member phase $NiCr_2S_4$.[16] It consists of ferromagnetic sheets parallel to the $(10\bar{1})$ planes with successive sheets antiferromagnetically coupled with respect to each other. The detailed structure differs slightly from that in which all moments, irrespective of cation site, lie parallel to the crystallographic *ab* plane, which was originally proposed for $NiCr_2S_4$ by Andron and Bertaut.[31] Rietveld analysis of low-temperature neutron diffraction data for $NiCr_2S_4$,[16] and for the vanadium-doped phases reported here, reveals that although the moments in the fully occupied layer are parallel to the *ab* plane, those in the vacancy layer lie in the *ac* plane directed at 140° to the [001] direction, a similar orientation to that of both the Cr(II) and Cr(III) moments in Cr_3S_4.[32] Magnetic susceptibility data indicate that the low-temperature magnetically ordered

(26) Powell, A. V.; Colgan, D. C.; Ritter, C. *J. Solid State Chem.* **1999**, *143*, 163.
(27) Bouchard, R. B.; Robinson, W. T.; Wold, A. *Inorg. Chem.* **1966**, *5*, 977.
(28) Elliot, S. R. In *The Physics and Chemistry of Solids*; Wiley: New York, 1998.
(29) Dijkstra, J.; van Bruggen, C. F.; Haas, C.; de Groot, R. A. *J. Phys.: Condens. Matter.* **1989**, *1*, 9163.
(30) Mott, N. F. In *Metal−Insulator Transitions*; Taylor & Francis: London, 1990.
(31) Andron, B.; Bertaut, E. F. *J. Phys. (Paris)* **1966**, *27*, 619.

state persists into the metallic phase and that there is a change from an antiferromagnetic insulator to an antiferromagnetic metal at $x \approx 0.6$. Vanadium doping decreases the Néel temperature (Figure 9), indicating a weakening of the magnetic interactions as the metallic phase is approached. The ordered moments at each of the two cation sites also decrease with increasing vanadium substitution (Figure 7), implying a decrease in the extent of electron localization. This may be a consequence of band broadening, associated with the increase in vanadium concentration in the fully occupied layer, which ultimately leads to the transition to a metallic phase. In the metallic phase, as the band broadens further, the moments and Néel temperature will tend to zero and magnetic order will disappear as is the case for $NiCr_{1.0}V_{1.0}S_4$, which low-temperature neutron diffraction reveals does not exhibit long-range magnetic order. This sequence of transitions from an antiferromagnetic insulator to an antiferromagnetic metal to a paramagnetic metal arising from an increase in B/U has been described by Mott[30] who also suggested that the observation of the antiferromagnetic metallic phase requires the change in the number of carriers at the electronic phase transition to be relatively small. Similar behavior, uncomplicated by the effects of changing the electron count, has been reported[33] for the series $NiS_{2-x}Se_x$ ($0 \leq x \leq 1.0$). In the present case, the magnetic susceptibility data for the paramagnetic metallic region reveal a degree of magnetic frustration which suggests that some local magnetic correlations persist until a truly paramagnetic metal appears at a composition $NiCr_{0.4}V_{1.6}S_4$.

In conclusion, $NiCr_{2-x}V_xS_4$ ($0 \leq x \leq 2$) provides an example of a series in which changes in chemical composition bring about an insulator to metal transition. Diffraction studies reveal that metallization is accompanied by a structural distortion, which results in zigzag chains of cations within the pseudo-hexagonal layer. However, as vanadium doping alters the position of the Fermi energy, introduces disorder into the fully occupied layer, and results in band broadening, the changes in magnetic and transport properties are likely to involve a complex interplay of several factors. Further study, including physical measurements on single crystals, are required in order to assess their relative importance.

Acknowledgment. The authors thank the EPSRC for a research grant in support of our neutron scattering program and The Leverhulme Trust for a research fellowship for P.V.

Supporting Information Available: Final, observed, calculated, and difference profiles, together with the refined structural parameters and bond lengths and angles for $NiCr_{2-x}V_xS_4$. This material is available free of charge via the Internet at http://pubs.acs.org.

CM990613E

(32) Bertaut, E. F.; Roult, G.; Aleonard, R.; Pauthenet, R.; Chevreton, M.; Jansen, R. *J. Phys. (Paris)* **1964**, *25*, 582.
(33) Honig, J. M.; Spalek, J. *Chem. Mater.* **1998**, *10*, 2910.